Neuron, Volume 77

Supplemental Information

Oligodendrocyte Dynamics in the Healthy Adult CNS:

Evidence for Myelin Remodeling

Kaylene M. Young, Konstantina Psachoulia, Richa B. Tripathi, Sara-Jane Dunn, Lee Cossell, David Attwell, Koujiro Tohyama, and William D. Richardson

1. Figure S1: Titrating EdU for in vitro and in vivo labelling. Related to Figure 1, main text.

2. Figure S2: Cumulative labelling with EdU in vivo. Related to Figure 1, main text.

3. Figure S3: Morphology of oligodendrocytes revealed by *Tau-mGFP* reporter mice.
Related to Figure 4, main text.

4. Figure S4. Counting internodes in thin sections: correction of sampling error.
Related to Figure 6, main text.

5. Methods.
Culturing OL lineage cells
Estimation of recombination efficiency in Pdgfra-CreER^{T2}: Tau-mGFP mice
Population dynamics and cell survival calculations
Simulations of myelinated axon action potential propagation
Primary and secondary antibodies for immuno-histochemistry

6. References

1. Figure S1: Titrating EdU for in vitro and in vivo labelling.

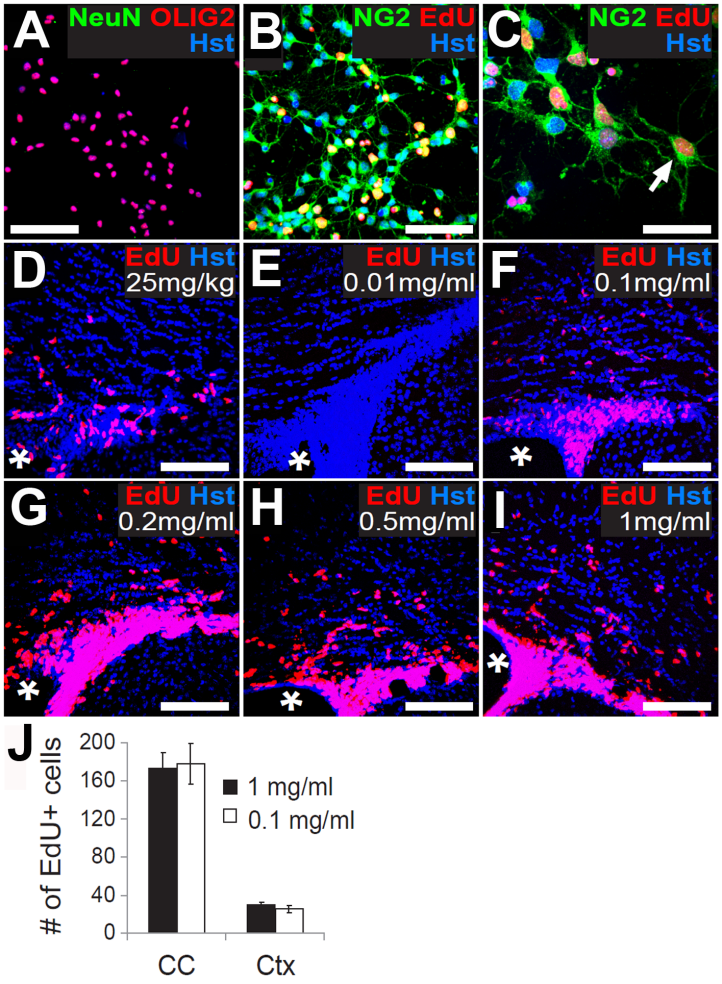

(**A**, **B**) Primary cultures of OPs from P15 cortex were grown in vitro for 24 hours before EdU was added to the medium. Cultures were fixed 18 hours later and (**A**) double-immunolabeled for NeuN (green) and Olig2 (red), or (**B**) immunolabeled for NG2 (green) and stained for EdU (red). (**C**) Higher magnification of (**B**). As expected under our culture conditions (see below methods), >99% of cells in the culture were Olig2$^+$ and none of them were NeuN$^+$. >99% of the cells were NG2$^+$ and approximately half of these were also EdU$^+$ (**D**) To label cells that are proliferating in vivo, EdU was administered to P21 mice by a single IP injection. EdU$^+$ cells (red) were detected within and outside the subventricular zone (SVZ). Having established the feasibility of in vivo labelling, we delivered EdU via the drinking water for 48 hours at a range of concentrations from 1 ng/ml to 1 mg/ml. (**E**) EdU was undetectable when administered at 0.01 mg/ml. (**F**-**I**) EdU$^+$ cells (red) were detected in the SVZ and parenchymal grey and white matter when EdU was used between 0.1 mg/ml and 1 mg/ml. (**J**) The number of EdU$^+$ cells detected in sections (30 µm thick) within a fixed area of corpus callosum (CC) (equivalent to 3 x 10^6 µm^3) or motor cortex (Ctx) (12 x 10^6 µm^3) was not different for mice exposed to 0.1 mg/ml or 1 mg/ml EdU for 48 hours. However labelling was visibly brighter at 0.2 mg/ml EdU and above (compare **F** with **G**-**I**). Sections were counterstained with Hoescht 33258 (blue) (Hst) to visualize cell nuclei. The location of the lateral ventricle is

indicated (*). Scale bars: 100 µm (**A**, **D**-**I**), 50 µm (**B**) or 15 µm (**C**).

2. Figure S2. Cumulative labelling with EdU in vivo

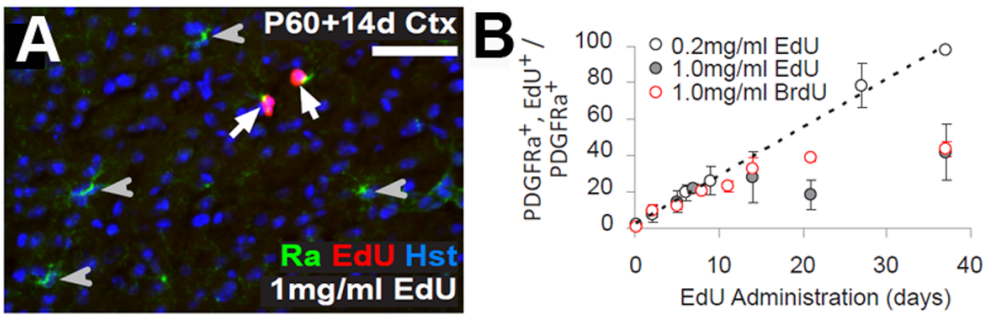

When mice were exposed to 1 mg/ml EdU in their drinking water for longer than 48 hours, there were clear signs of toxicity. In one experiment with three P21 mice, one died after 13 days exposure (P21+13) and the other two developed hunched posture and were humanely killed. In a second experiment with twelve P60 mice, one died on P60+13 and two developed hunched posture; the other nine appeared normal throughout the treatment period (up to 37 days). No lethality or altered posture was observed with 0.2 mg/ml EdU, even when it was provided for 50 days (P60+50).

Dividing OPs were labelled by continuous administration of EdU (0.2 mg/ml or 1 mg/ml) or BrdU (1 mg/ml) to P60 mice via their drinking water for up to 37 days. At various labelling periods, coronal brain sections were immunolabelled for Pdgfra (green) and processed to detect EdU (red, **A**), or immunolabelled for BrdU. (**B**) The fraction of Pdgfra$^+$ OPs in the cerebral cortex that was labelled for EdU or BrdU (labelling index, %) was plotted against labelling time. When EdU or BrdU was given at 1 mg/ml, the labelling index did not rise above ~40%. However, when EdU was given at 0.2 mg/ml the labelling index rose to ~100%. We conclude that EdU or BrdU at 1 mg/ml has a toxic effect that inhibits cells entering or progressing through S-phase and leads to an erroneously low labelling index. These data indicate that even mice that did not display outward symptoms of EdU-toxicity still experienced adverse effects on cell proliferation/ EdU labeling during prolonged exposure to 1 mg/ml EdU. Therefore 0.2 mg/ml EdU was used subsequently.

3. Figure S3: Morphology of oligodendrocytes revealed by *Tau-mGFP* reporter mice

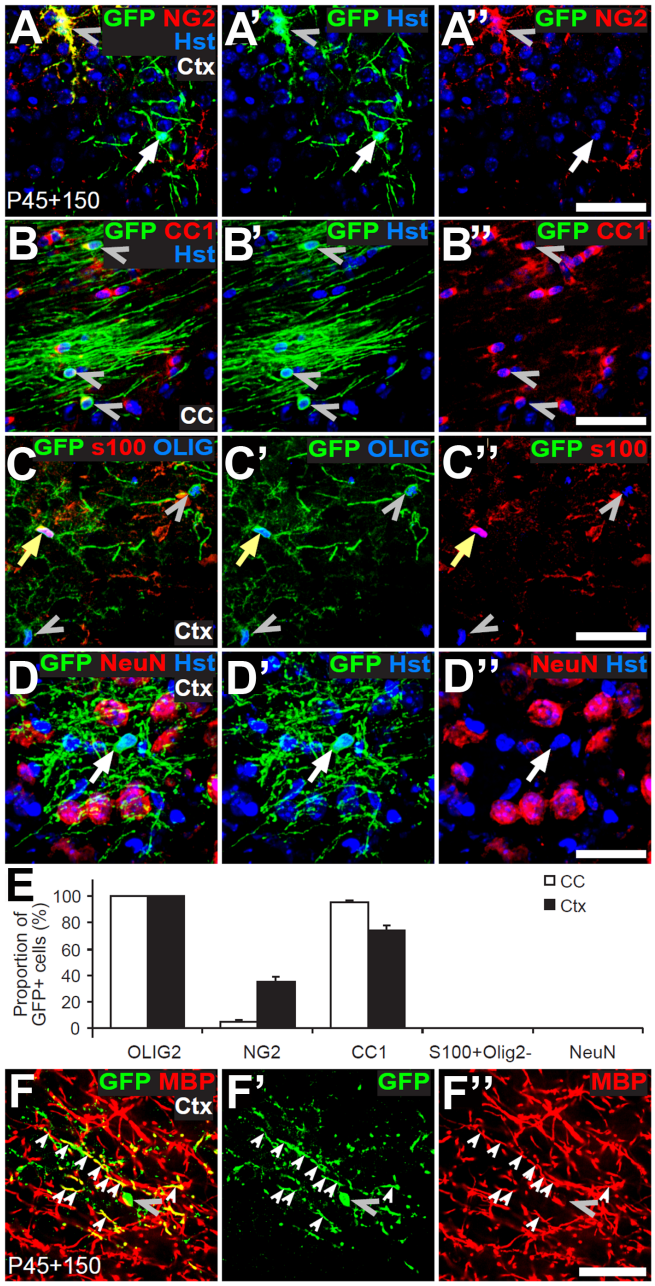

Tamoxifen was administered to P45 *Pdgfra-CreER^{T2} : Tau-mGFP* mice and the morphologies of mGFP^{+} cells in both the corpus callosum and motor cortex were examined at P45+150. mGFP^{+} cells in the corpus callosum had small, spherical cell bodies with numerous rod-like processes that ran parallel to each other in the direction of the axons (**B**). In the motor cortex, the cell processes were less dense, less numerous and randomly oriented but myelin profiles were still evident (**A, C, D, F**). The identity of the mGFP^{+} cells in *Pdgfra-CreER^{T2} : Tau-mGFP* mice following tamoxifen administration (P45+150) was confirmed by immunolabeling for NG2, APC/ CC1, Olig2, S100ß and NeuN in various combinations. We did not find any mGFP^{+} cells that were S100ß$^{+}$, Olig2-negative (**C, E**), which was as expected because astrocytes do not express Tau and in any case adult OPs do not normally generate astrocytes (reviewed by Richardson et al., 2011).

Similarly, mGFP$^+$ cells in the motor cortex and corpus callosum were negative for NeuN, demonstrating that OPs do not generate neurons in those regions (**D, E**). All mGFP$^+$ cells were also Olig2$^+$, indicating that they all belonged to the OL lineage (**C, E**). Of the mGFP$^+$ cells in the corpus callosum, a small proportion (~5%) expressed the OP marker NG2 but these cells had the lowest levels of mGFP expression, suggesting that they corresponded to the most recently formed OLs that had not yet lost NG2 (**E**). The proportion of YFP$^+$ cells that was NG2$^+$ was greater in the motor cortex (~35%) (**A, E**), consistent with previous reports that the time course of OL differentiation is more protracted in the cortical grey matter (Dimou et al., 2008; Kang et al., 2010). The majority of mGFP$^+$ cells co-labelled with the OL-specific antibody CC1, both in the corpus callosum (~96% of mGFP$^+$ cells were CC1$^+$) and in the motor cortex (~75% of mGFP$^+$ cells were CC1$^+$) (**B, E**). In addition, the cytoplasmic processes of mGFP$^+$ cells, including the non-aligned mGFP$^+$ processes in the motor cortex (**F**), were found to align with myelin basic protein (MBP)-positive internodes.

4. Figure S4. Counting internodes in thin sections: correction of sampling error.

We counted the number of internodes per recently-formed (GFP$^+$) oligodendrocyte (OL) in thin (30 µm) longitudinal sections of *Pdgfra-CreER^{T2} : Tau-mGFP* optic nerves. An individual OL resembles a loose "bundle of sticks" in which each "stick" represents an internode. The cross-sectional profile of the bundle is roughly circular so that the whole bundle has a roughly cylindrical shape, with the cell body at its center. If we cut sections along the long axis of this cylinder, paying attention only to those sections that contain the cell body, then the diameter of the cylinder can be measured in side view. Since in practice our section thickness T (30 µm) is less than the cylinder diameter $2r$ (~40-60 µm), only part of the OL is contained within the section. Therefore the number of internodes visible in the section is less than the "true" number, i.e. there is a sampling error. Assuming that the long axis of the cylinder (the direction of retinal ganglion cell axons) is aligned with the plane of section, then the fraction of the cylinder volume that is contained in the section is the same as the fractional cross-sectional area $A_S/\pi r^2$, where πr^2 is the cross-sectional area of the cylinder and A_S that part of the area that is contained within the section (i.e. $[\pi r^2 - (A + B)]$ in **Fig. S4**). If a collection of identical aligned cylinders is sectioned so that their centers are randomly positioned within the section, we can derive a general expression for the mean cross-sectional area $\overline{A_S}$ of the collection of cylinders and hence calculate a correction factor to scale the number of internodes that we count in the section to the "correct" value.

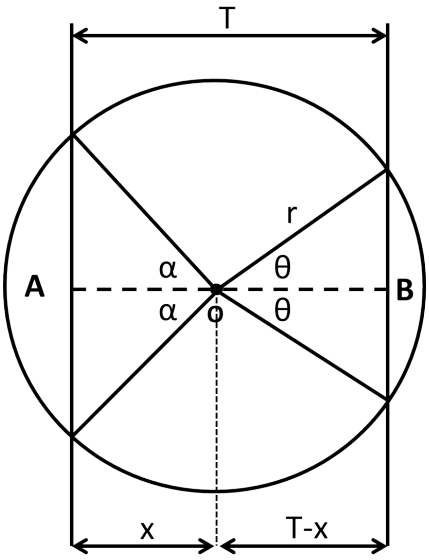

Figure S4. We want to determine the cross-sectional area of the circular face that lies within a strip of width T, which is illustrated here for the general case of the strip sitting asymmetrically about the center of the circle. The center of the circle is constrained to lie within the strip, but only one edge of the strip may lie outside the circle boundary, if $2r > T > r$.

To calculate the area of the overlap between strip and circle, we can either subtract the area of segments A and B from the total area of the circle of radius r, or we can sum the areas of the two triangles (one of angle 2α, the other of angle 2θ) and the two remaining sectors [each of radius r and angle $\pi - (\alpha + \theta)$] within the strip.

Consider the general case where the strip does not lie symmetrically about the cell body, which is the center of the circle, $\boldsymbol{O}$. We define the distance from $\boldsymbol{O}$ to the left edge of the strip to be x, and therefore the distance from $\boldsymbol{O}$ to the right edge is $(T - x)$.

If we assume that if the strip does not contain the center $\boldsymbol{O}$ it is disregarded from the experiments, then $x \geq 0$. There are then two cases to consider for the area of overlap of circle and strip, A_s :

1. $(T - x) < r \Rightarrow A_s = r^2(\pi - \theta - \alpha) + (T - x)\sqrt{r^2 - (T - x)^2} + x\sqrt{r^2 - x^2}$ the general case when both edges of the strip lie within the circle as depicted in **Fig. S4**.

2. $(T - x) \geq r \Rightarrow A_s = r^2(\pi - \alpha) + x\sqrt{r^2 - x^2}$ when one edge of the strip lies outside the circle and the other inside (so $\theta \to 0$). In the special case when one edge of the strip is outside the circle and the other edge passes through $\boldsymbol{O}$ ($x = 0$, $\theta \to 0$ and $\alpha \to \pi/2$), the formula reduces to $A_s = \pi r^2/2$ (the area of a hemicircle).

To get the average strip area over all allowed values of x we consider

$$\overline{A_s} = \frac{\int_0^T A_s\, dx}{T},$$

and given that A_s is continuous on $[0, T]$, by symmetry:

$$\frac{1}{T}\int_0^T A_s\, dx = \frac{2}{T}\int_0^{T/2} A_s\, dx\,.$$

In our experiments, $2r > T > r$, so we consider two separate integrals:

$$\frac{2}{T}\int_0^{T/2} A_s\, dx = \frac{2}{T}\int_0^{T-r} r^2(\pi - \alpha) + x\sqrt{r^2 - x^2}\, dx + \frac{2}{T}\int_{T-r}^{T/2} r^2(\pi - \theta - \alpha) + (T-x)\sqrt{r^2 - (T-x)^2} + x\sqrt{r^2 - x^2}\, dx. \quad (1)$$

From **Fig. S4**,

$$\theta = \cos^{-1}\left(\frac{T-x}{r}\right),$$

$$\alpha = \cos^{-1}\left(\frac{x}{r}\right),$$

and by standard trigonometry,

$$\int \cos^{-1}(x)dx = x\cos^{-1}(x) - \sqrt{1-x^2} + C\,,$$

where C is constant.

By the substitution $y = (T-x)/r$,

$$\int \cos^{-1}\left(\frac{T-x}{r}\right)dx = \int -r\cos^{-1}(y)dy = -r\left(y\cos^{-1}(y) - \sqrt{1-y^2} + C\right)$$
$$= -r\left(\left(\frac{T-x}{r}\right)\cos^{-1}\left(\frac{T-x}{r}\right) - \sqrt{1-\left(\frac{T-x}{r}\right)^2} + C\right).$$

Similarly,

$$\int \cos^{-1}\left(\frac{x}{r}\right)dx = x\cos^{-1}\left(\frac{x}{r}\right) - \sqrt{r^2-x^2} + C\,.$$

The remaining terms in the integrals in (1) are calculated as follows. Given that

$$\frac{d}{dx}\left((r^2-x^2)^{\frac{3}{2}}\right) = -3x\sqrt{r^2-x^2},$$

it follows that

$$\int x\sqrt{r^2-x^2}dx = -\frac{(r^2-x^2)^{\frac{3}{2}}}{3} + C.$$

Similarly,

$$\int (T-x)\sqrt{r^2-(T-x)^2}dx = \frac{(r^2-(T-x)^2)^{\frac{3}{2}}}{3} + C.$$

Now it is possible to solve each integral in (1) individually. First,

$$\frac{2}{T}\int_0^{T-r} r^2(\pi-\alpha) + x\sqrt{r^2-x^2}\,dx = \left[r^2\pi x - r^2 x\cos\left(\frac{x}{r}\right) + \sqrt{r^2-x^2} - \frac{(r^2-x^2)^{\frac{3}{2}}}{3}\right]_0^{T-r} \quad (2)$$

and second,

$$\frac{2}{T}\int_{T-r}^{T/2} r^2(\pi-\theta-\alpha) + (T-x)\sqrt{r^2-(T-x)^2} + x\sqrt{r^2-x^2}dx$$
$$= \left[r^2\pi x + r^2(T\right.$$
$$\left. - x)\cos^{-1}\left(\frac{T-x}{r}\right) - r^2\sqrt{r^2-(T-x)^2} - r^2 x\cos\left(\frac{x}{r}\right) - r^2\sqrt{r^2-x^2} + \frac{(r^2-(T-x)^2)^{\frac{3}{2}}}{3}\right.$$
$$\left. - \frac{(r^2-x^2)^{3/2}}{3}\right]_{T-r}^{T/2}. \quad (3)$$

By evaluating the right-hand side of equations (2) and (3) according to the limits of the definite integrals, following

$$\int_a^b f'(x)dx = [f(x)]_a^b = f(b) - f(a),$$

where $df(x)/dx = f'(x)$. By summing according to (1), many of the terms cancel to give:

$$\overline{A_s} = \frac{2}{T}\int_0^{T/2} A_s dx = \pi r^2 - \frac{4r^3}{3T}.$$

This is a general expression for the mean cross-sectional area, $\overline{A_s}$, for $(2r > T > r)$. It follows that the mean fractional volume of the cylinder that is contained within the section is $\overline{A_s}/\pi r^2$. Therefore, we must multiply our internode counts by a correction factor: $\pi r^2/\overline{A_s} = 3\pi T/(3\pi T - 4r)$, to give an estimate of the actual number of internodes per OL. For example, for $r = 27.5\ \mu\text{m}$, $T = 30.0\ \mu\text{m}$, the correction factor is 1.64.

5. Methods

Culturing OL lineage cells

P15 mice were killed by cervical dislocation. Brains were removed into Earle's Buffered Saline Solution without $Ca2^+$ or $Mg2^+$ (EBSS; Invitrogen), the olfactory bulbs were removed and the region caudal to the optic chiasm was discarded. Forebrain cortical tissue was dissected and incubated at 37^{o}C for 45 minutes in EBSS containing 62.5 ng/ml Trypsin (Sigma) and 56.25 ng/ml DNase I (Sigma). Dulbecco's Modified Eagle's Medium (DMEM) containing 10% (v/v) fetal calf serum (FCS) was added to inactivate the trypsin and the tissue was dissociated by gentle agitation (Pringle et al., 1996). Cells were resuspended in DMEM/10% FCS containing 10 pM basic fibroblast growth factor (Invitrogen) and passed through a 70 µm cell sieve (Falcon). Cells were then plated on poly-D-lysine (Sigma) coated glass coverslips in 24 well tissue culture plates (Falcon) at a concentration of $1.5x10^5$ cells/well in SATO medium optimized for postnatal cultures (Cahoy et al., 2008). Cells were cultured for up to 48 hours in a humid incubator at 37ºC in a 5% (v/v) CO_2 atmosphere.

Estimation of recombination efficiency in Pdgfra-CreER^{T2}: Tau-mGFP mice

In *Pdgfra-CreER^{T2} : Tau-mGFP* mice, recombination occurs in OPs under the control of *Pdgfra-CreER^{T2}* but mGFP is not expressed until the OPs differentiate into OLs and the *Tau-mGFP* reporter becomes transcriptionally active. Therefore we cannot compare recombination efficiencies of *Tau-mGFP* and *R26R-YFP* directly in OPs. Instead, we compared their recombination efficiencies by counting mGFP- or YFP-labelled neurons in the piriform cortex of *Pdgfra-CreER^{T2} : Tau-mGFP* versus *Pdgfra-CreER^{T2} : R26R-YFP* mice (Rivers et al., 2008). 150 days after administering tamoxifen to P60 mice there were 24 fluorescently labelled neurons in a selected area of *R26R-YFP* piriform cortex and 5 in *Tau-mGFP*, so the efficiency of recombination in *Tau-mGFP* is ~21% that in *R26R-YFP* using the same Cre driver. Since the recombination efficiency in OPs of *Pdgfra-CreER^{T2} : R26R-YFP* optic nerves is ~20% (see main text, Results), we infer that the recombination efficiency of *Pdgfra-CreER^{T2} : Tau-mGFP* in optic nerve OPs is ~4% - i.e. 4% of all $Pdgfra^+$ OPs in the nerve recombine the reporter.

Population dynamics and cell survival calculations

The fraction of OPs that label with EdU ("labelling index") increases linearly with the duration of EdU exposure until all dividing cells are labelled (phase 1) and a plateau is reached (phase 2). The rate at which cells incorporate EdU is given by the slope (*m*) of phase 1. The maximum labelling index (phase 2 plateau value) is known as the "growth fraction" (*GF*), which is the fraction of the total cell population that is capable of entering S-phase. From these data we calculated the length of the cell cycle (T_C) = *GF/m* and the length of S-phase (T_S) = y-intercept (i.e. labelling index

at t=0) */m* (Nowakowski et al., 1989). Statistical analyses were as previously described (Psachoulia et al., 2009).

T_C *is* proportional to age in cerebral cortex up to at least P500 and approximately so in corpus callosum up to ~P240 (Psachoulia et al., 2009). Therefore, we can write $T_C = T_0 + rt$ where T_0 is the cell cycle time at the start of the experiment (time of tamoxifen administration), t the age of the animal and r the rate of increase of T_C with t (determined experimentally to be ~0.61 for the cortex, ~0.17 for the corpus callosum, ~0.32 for optic nerve) (see main text, **Table 1**). Following tamoxifen administration to label a proportion of OPs in *Pdgfra-CreER^{T2}: R26R-YFP* mice, differentiated OLs start to accumulate at a rate $dN/dt = p/T_C = p/(T_0+rt)$ where p is the number of labelled OPs, which remains approximately constant throughout postnatal life (Rivers et al., 2008). Integrating over the time course of the experiment and assuming no cell death, we find that the accumulated number of differentiated OLs is $N = (p/r).\ ln(1+rt/T_0)$. From this we calculate the ratio of differentiated OLs to all OL lineage cells, i.e. the fraction F of all YFP$^+$ cells (OLs + OPs) that are CC1$^+$ OLs [(YFP$^+$, CC1$^+$)/ YFP$^+$] = $ln(1+rt/T_0)/\ [r + ln(1+rt/T_0)]$. The experimentally determined value will be less than the calculated value if there is significant death of newly-formed OLs. For example, in the P60+42 corpus callosum, T_0 = 9.5 days so from the above F = 77%, whereas by experiment we measure $F(expt)$ = 50%. If n is the predicted number of OLs, m the actual number of surviving OLs, then $n/(n+p)$ = 0.77 and $m/(m+p)$ = 0.5, from which we deduce that n = (0.77/0.23)p and $m = p$, hence the fraction of surviving OLs m/n = 0.23/0.77 = 30%.

Simulations of myelinated axon action potential propagation

The myelinated axon model C of Richardson et al. (2000) was implemented in MATLAB, as described by Bakiri et al. (2011) for 37^{o}C, but with all specific capacitances set to 1 mF/cm^2, a specific myelin membrane conductance of 1 mS/cm^2, a node length of 0.8 μm (Ishibashi et al., 2002), an axon diameter of 0.524 μm (as measured, see main text) and a g-ratio of 0.753 which corresponds to six myelin wraps. The internode length was set to 138 μm or 22 μm to simulate early- or late-born internodes and the periaxonal space width was set to zero (by setting its conductivity to zero) or to 3 nm with a resistivity of 0.7 μΩ-m as described in the main text. The differential equations of the model were derived and solved according to the method used in Halter and Clark (1991). Fifty-one internodes were simulated and the conduction speed was derived from the time needed for the action potential to pass from the 20th to the 30th internode. The conduction speed predicted for 138 μm long internodes with no periaxonal space (1.83 m/s) was in reasonable agreement with the values (1.8-3.7 m/s depending on axon size) measured for mouse optic nerve by Devaux and Gow (2008).

Primary and secondary antibodies for immuno-histochemistry

Primary antibodes used in this study were: rat monoclonal anti-Pdgfra (1:300, BD Pharmingen™), rabbit anti-GFP (1:1000, Synaptic Systems), rat anti-GFP (1:3000, BD Pharmingen™), mouse anti-adenomatous polyposis coli (monoclonal CC1: 1:200, Calbiochem), rabbit anti-NG2 (1:500, Millipore), rabbit anti-Olig2 (1:1000, Millipore), mouse anti-s100β (1:1000, Sigma), mouse anti-NeuN (1:500, Millipore), rabbit anti-NaV1.6 (1:200, Alamone Labs) and mouse anti-Caspr, clone K65/35 (1:100, UC Davis/ NIH Neuromab). Secondary antibodies were: goat anti-rat (1:500), donkey anti-rabbit (1:1000), goat anti-mouse IgG1 (1:1000) or goat anti-mouse IgG (heavy and light chains) (1:1000) conjugated to Alexa Fluor-488, -568, or -647 (Invitrogen). When immunolabelling with monoclonal CC1, Tris-buffered saline (TBS) blocking solution (0.5% [v/v] Triton-X100 and 10% FCS in TBS) was used in place of PBS blocking solution and all washes were in TBS

6. References

Bakiri, Y., Karadottir, R., Cossell, L., and Attwell, D. (2011). The morphological and electrical characteristics of oligodendrocytes in the developing white matter of the corpus callosum and cerebellum. J. Physiol. *589*, 559-573.

Cahoy, J.D., Emery, B., Kaushal, A., Foo, L.C., Zamanian, J.L., Christopherson, K.S., Xing, Y., Lubischer, J.L., Krieg, P.A., Krupenko, S.A., Thompson, W.J., and Barres, B.A. (2008). A transcriptome database for astrocytes, neurons, and oligodendrocytes: a new resource for understanding brain development and function. J. Neurosci. *28*, 264-278.

Devaux, J., and Gow, A. (2008). Tight junctions potentiate the insulative properties of small CNS myelinated axons. J. Cell Biol. *183*, 909-921.

Dimou, L., Simon, C., Kirchhoff, F., Takebayashi, H., and Götz, M. (2008). Progeny of Olig2-expressing progenitors in the gray and white matter of the adult mouse cerebral cortex. J. Neurosci. *28*, 10434-10442.

Halter, J.A. and Clark, J.W. Jr. (1991). A distributed-parameter model of the myelinated nerve fiber. J. Theor. Biol. *148*, 345-382.

Ishibashi, T., Dupree, J.L., Ikenaka, K., Hirahara, Y., Honke, K., Peles, E., Popko, B., Suzuki, K., Nishino, H., and Baba, H. (2002). A myelin galactolipid, sulfatide, is essential for maintenance of ion channels on myelinated axons but not essential for initial cluster formation. J. Neurosci. *22*, 6507-6514.

Kang, S.H., Fukaya, M., Yang, J.K., Rothstein, J.D., and Bergles, D.E. (2010). $NG2^+$ CNS glial progenitors remain committed to the oligodendrocyte lineage in postnatal life and following neurodegeneration. Neuron *68*, 668-681.

Nowakowski, R.S., Lewin, S.B., and Miller, M.W. (1989). Bromodeoxyuridine immunohistochemical determination of the lengths of the cell cycle and the DNA-synthetic phase for an anatomically defined population. J. Neurocytol. *18*, 311-318.

Pringle, N.P., Yu, W.P., Guthrie, S., Roelink, H., Lumsden, A., Peterson, A.C., and Richardson, W.D. (1996). Determination of neuroepithelial cell fate: induction of the oligodendrocyte lineage by ventral midline cells and sonic hedgehog. Dev. Biol. *177*, 30-42.

Psachoulia, K., Jamen, F., Young, K.M., and Richardson, W.D. (2009). Cell cycle dynamics of NG2 cells in the postnatal and ageing brain. Neuron Glia Biol. *5*, 57-67.

Richardson, A.G., McIntyre, C.C., and Grill, W.M. (2000). Modelling the effects of electric fields on nerve fibres: influence of the myelin sheath. Med. Biol. Eng. Comput. *38*, 438-446.

Richardson, W.D., Young, K.M., Tripathi, R.B., and McKenzie, I. (2011). NG2-glia as Multipotent Neural Stem Cells: Fact or Fantasy? Neuron *70*, 661-673.

Rivers, L.E., Young, K.M., Rizzi, M., Jamen, F., Psachoulia, K., Wade, A., Kessaris, N., and Richardson, W.D. (2008). PDGFRA/NG2 glia generate myelinating oligodendrocytes and piriform projection neurons in adult mice. Nat. Neurosci. *11*, 1392-1401.